Exotic colored fermions and lepton number violation at the LHC

E. Carquin* and N. A. Neill†
Departamento de Física y CCTVal Universidad Técnica Federico Santa María, Casilla 110-V, Valparaíso, Chile

J. C. Helo‡
Departamento de Física y Astronomía, Facultad de Ciencias, Universidad de La Serena, Avenida Cisternas 1200, La Serena, Chile

M. Hirsch§
AHEP Group, Instituto de Física Corpuscular-CSIC/Universitat de València Parque Científico, C/Catedrático José Beltrán, 2, E-46980 Paterna, Spain

(Received 21 April 2019; published 21 June 2019)

Majorana neutrino mass models with a scale of lepton number violation of order tera-electron-volts potentially lead to signals at the LHC. Here, we consider an extension of the standard model with a colored octet fermion and a scalar leptoquark. This model generates neutrino masses at two-loop order. We make a detailed Monte Carlo study of the lepton number violating signal at the LHC in this model, including a simulation of standard model backgrounds. Our forecast predicts that the LHC with 300/fb should be able to probe this model up to color-octet fermion masses in the range of (2.6–2.7) TeV, depending on the lepton flavor of the final state.

DOI: 10.1103/PhysRevD.99.115028

I. INTRODUCTION

All Majorana neutrino mass models with a scale of lepton number violation (LNV) of roughly $\Lambda_{\rm LNV} \sim \mathcal{O}$ (TeV) can lead to lepton number violating signals at the LHC. The best-known example is the left-right symmetric extension of the standard model [1–3]. Here, right-handed W_R boson production can lead to the final states $\ell^\pm\ell^\pm jj$ and $\ell^\pm\ell^\mp jj$ [4].[1]

There are, however, many other possible electroweak scale extensions of the standard model that potentially lead to LNV signals at the LHC. In particular, the systematic analysis of the short-range contributions to neutrinoless double beta decay [6] has found a variety of such models, all of which can in principle explain neutrino oscillation data. (For a recent global fit of all oscillation data, see, e.g., Ref. [7].) Rough estimates of the LHC reach, compared with the sensitivity of current and future double beta decay experiments, have been made in Refs. [8–10]. In this paper, we study LHC signals for a particularly simple LNV extension of the standard model (SM). This model generates neutrino masses at two-loop order, and, thus, one expects the masses of the exotic particles of this model to be at least partially within reach of the LHC. We mention that a one-loop neutrino mass model with colored particles has been discussed in Ref. [11]; its LHC phenomenology was studied in Ref. [12]. Differently from previous papers [8–10], here we perform a full detector simulation and background study, in order to give more realistic estimates for future LHC sensitivities.

Only very few searches for LNV final states at the LHC exist so far. CMS [13] has searched for same-sign dileptons plus jets in 8 TeV data. The results were interpreted as lower limits on the mass of W_R as function of right-handed neutrino mass. Lower limits on m_{W_R} approaching 3 TeV have been derived, for $m_N < m_{W_R}$ and assuming the gauge coupling of the right-handed bosons to be equal to the standard model $SU(2)_L$ coupling. A small excess around $p^2_{\ell\ell jj} = 2$ TeV was observed (statistically with a local significance of 2.8σ) but discarded by the experimentalists as a signal, since the sample consists dominantly of opposite-sign lepton final states. (See, however, the discussion in Ref. [14].) Unfortunately, the recent update of

*edson.carquin@usm.cl
†nicolas.neill@gmail.com
‡jchelo@userena.cl
§mahirsch@ific.uv.es

[1]For a recent study of the LHC phenomenology of left-right symmetry, see, e.g., Ref. [5].

this search by CMS [15] with $\sqrt{s} = 13$ TeV data could not reproduce this excess and now quotes a lower limit of $m_{W_R} \geq 4.4$ TeV. A very similar search by ATLAS [16] has also been published, providing lower limits extending up to $m_{W_R} \geq 4.7$ TeV, for $m_N \lesssim m_{W_R}/2$.

We also want to mention that for models with a seesaw type II, pair production of the doubly charged component of the triplet can lead to $\Delta^{++}\Delta^{--} \to \ell^{\pm}\ell^{\pm}W^{\mp}W^{\mp} \to \ell^{\pm}\ell^{\pm} + 4j$ [17–19].[2] If only leptonic or WW final states were observed, LNV could not be established at the LHC, but the type of scalar multiplet could still be determined [20]. However, no search for $\ell^{\pm}\ell^{\pm}W^{\mp}W^{\mp}$ at the LHC exists so far. Instead, ATLAS [21] searched for $pp \to \Delta^{++}\Delta^{--} \to 4\ell$. For a doubly charged Higgs boson only coupling to left-handed leptons, the limits vary from (770–870) GeV, depending on the lepton flavor, assuming $\mathrm{Br}(\Delta^{\pm\pm} \to \ell^{\pm}_{\alpha}\ell^{\pm}_{\beta})$ equal to 1 (for $\alpha, \beta = e, \mu$). ATLAS [22] has also searched for $pp \to \Delta^{++}\Delta^{--} \to 4W$. However, lower limits, based on 36.1/fb, are currently only of order 220 GeV.

The model we consider in this paper contains two new particles: a scalar leptoquark (LQ) and an exotic color-octet fermion, Ψ (for details, see Sec. II). The fermion can be pair produced, decaying to the final state $\ell^{\pm}jj$. We will discuss restrictions on the fermion in this model from the searches [15,16] in Sec. IV. As for the leptoquark, currently the best limits come from CMS [23] and ATLAS [24]. CMS [23] finds lower limits on pair-produced leptoquarks, giving $m_{\mathrm{LQ}} \geq 1435$ (1270) GeV for a branching ratio of $\mathrm{Br}(S_{\mathrm{LQ}} \to \ell^{\pm}j) = 1$ (0.5). ATLAS derives [24] a very similar number of $m_{\mathrm{LQ}} \geq 1.25$ TeV for a branching ratio equal to 0.5.

In order to estimate the reach of our model for the LHC Run 3, we performed detector level studies of the same-sign dilepton plus four jets final state. In Sec. III, the Monte Carlo simulation and the cut and count analysis optimization are discussed in some detail. Signal and SM background H_T distributions are shown, and the corresponding yield tables after the selection cuts are included for completeness in the Appendix. In Sec. IV, our results are presented as the 2σ limits and 5σ discovery regions, forecasted for the $\Psi \to \ell^{\pm}jj$ branching ratio, with $\ell = e, \mu$, as a function of the color-octet fermion mass.

The rest of this paper is organized as follows. In Sec. II, we describe the model basics; discuss briefly non-LHC constraints, such as neutrino masses; and describe the benchmark scenarios we use in the rest of the paper. In Sec. III, the Monte Carlo simulation is discussed, and our results are presented in Sec. IV. In Sec. V, the conclusions and outlook of this work are given.

[2]To establish LNV experimentally, one needs to study final states *without* missing energy.

II. MODEL BASICS

In this paper, we use a particularly simple two-loop neutrino mass model. The model adds only two new particles to the standard model: a (singlet) scalar leptoquark $S_{\mathrm{LQ}} \equiv S_{3,1,-1/3}$ and a color octet fermion, $\Psi \equiv \Psi_{8,1,0}$. Here, the subscripts denote the transformation properties/charge under the SM gauge group, $SU(3)_c \times SU(2)_L \times U(1)_Y$. We note that this model has appeared twice in the literature before. It was listed in Ref. [6][3] as one particular example of a short-range contribution to neutrinoless double beta decay. And in Ref. [26], predictions for neutrino masses and low energy lepton flavor violation for this model have been worked out in detail.

With these new fields, the Lagrangian of the model contains the following terms:

$$\begin{aligned}\mathcal{L} = {} & (Y_1)_{\alpha\beta}\overline{L^c}_{\alpha}Q_{\beta}S^{\dagger}_{\mathrm{LQ}} + (Y_2)_{\alpha\beta}\overline{d_R}_{\alpha}\Psi_{\beta}S_{\mathrm{LQ}} \\ & + (Y_3)_{\alpha\beta}\overline{e^c_R}_{\alpha}u_{R\beta}S^{\dagger}_{\mathrm{LQ}} + \mathrm{H.c.} \\ & + \frac{1}{2}m_{\Psi}\bar{\Psi}^c\Psi + m^2_{\mathrm{LQ}}S^{\dagger}_{\mathrm{LQ}}S_{\mathrm{LQ}} + \cdots \end{aligned} \tag{1}$$

Here, α and β are generation indices, and we have left open the possibility that more than one copy of Ψ could exist. The quantum numbers of the scalar leptoquark S_{LQ} allow us, in principle, to write down two more terms in the Lagrangian, $\bar{Q}Q^cS_{\mathrm{LQ}}$ and $\bar{u}d^cS^{\dagger}_{\mathrm{LQ}}$. These, if coupled to the first generation of quarks, induce rapid proton decay. As noted in Ref. [27], stringent upper limits on Yukawa couplings in any quark generation indices can be derived from the requirement of successful baryogenesis. In order to avoid these problems, we simply postulate baryon number conservation as an additional symmetry of the model.

The main motivation for studying this model is that it can explain neutrino oscillation data by generating neutrino masses at two-loop level as shown in Fig. 1. Assuming only one copy of Ψ, this diagram gives a contribution to the neutrino mass matrix, roughly as [26,28,29]

$$\begin{aligned}(m_{\nu})_{\alpha\beta} \sim {} & \frac{N_c}{(16\pi^2)^2}\frac{m_{\Psi}}{m^2_{\mathrm{LQ}}}[(Y_1)_{\alpha k}(Y_2)_k m_k I_{kr}(x^2) \\ & \times m_r(Y_2)_r(Y_1)_{\beta r} + \alpha \leftrightarrow \beta]. \end{aligned} \tag{2}$$

Here, N_c is a color factor; m_k and m_r are down quark masses of generation k, r; and $I_{kr}(x^2)$ stands for the two-loop integral [26,29], with the dimensionless argument $x = (m_{\Psi}/m_{\mathrm{LQ}})$. Note that with the quark masses much smaller than the mass of Ψ and S_{LQ}, $I_{kr}(x^2)$ is to a good approximation independent of k and r, i.e., $I(x^2)$. In order to reproduce the neutrino mass, estimated from the atmospheric neutrino mass scale ($m_{\nu} \sim 0.05$ eV) and assuming

[3]Decomposition T-I-5-i for the Babu-Leung operator #11 [25].

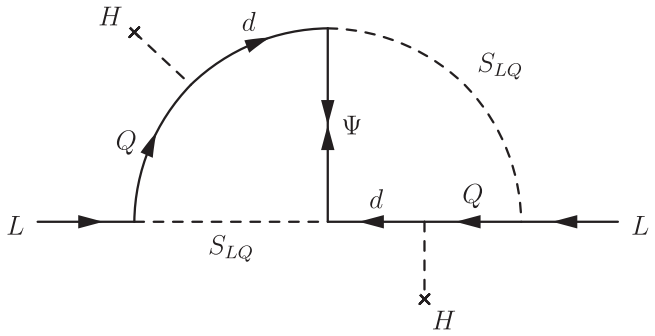

FIG. 1. Two-loop neutrino mass diagram for the model considered in this work.

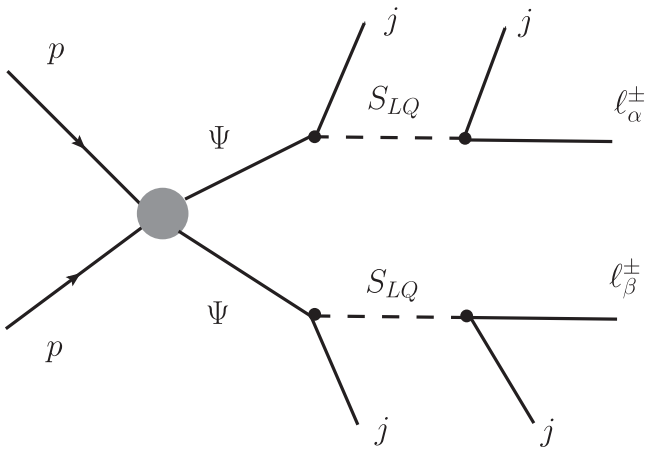

FIG. 2. Pair production of the color-octet fermion Ψ, followed by three-body decays, at the LHC.

very roughly $m_\Psi \sim m_{\rm LQ} \sim \Lambda_{\rm LNV} \sim \mathcal{O}$ (TeV), the Yukawa couplings (for third generation quarks) in Eq. (2) should be of order (few) $\mathcal{O}(10^{-2})$.

Since neutrino mass models must not only produce the correct absolute value of one neutrino mass but also reproduce the solar mass scale and the observed flavor structure of the neutrino mass matrix, the above estimate is only indicative of the typical size of parameters. On closer inspection, one sees that in the limit where only m_b is taken different from zero, Eq. (2) generates only one neutrino mass. The authors of Ref. [26] therefore suggested using two copies of $S_{\rm LQ}$. However, we note that contributions proportional to m_s, while being smaller than those proportional to m_b, could generate a large enough second neutrino mass, if the entries in the Yukawa matrices Y_1 and Y_2 for second generation quarks are roughly larger, by a factor $\sqrt{m_b/m_s} \sim 6$ each, than those for third generation quarks. Also, the fit of nonzero neutrino angles requires flavor off-diagonal entries in $(m_\nu)_{\alpha\beta}$, implying lepton flavor violating charged lepton decays. We will not repeat this discussion here, since a detailed study can be found in Ref. [26].

Lepton number violation in this model is due to the Majorana mass term m_Ψ. Ψ, once produced, can decay to a down quark and $S_{\rm LQ}$. Since Ψ is a Majorana fermion, decays to $\overline{d_R} S_{\rm LQ}$ and $d_R S_{\rm LQ}^\dagger$ are equally likely. Thus, pair-produced Ψ will lead to the LNV and lepton number conserving final states $\ell_\alpha^\pm \ell_\beta^\pm + 4j$ and $\ell_\alpha^\pm \ell_\beta^\mp + 4j$, as shown in Fig. 2. There are, however, some important differences to the case of the type-II seesaw discussed in the Introduction. First, Ψ being a color octet, production cross sections are much larger in the current model. And, second, in type-II seesaw, the invariant masses of the subsystems $\ell_\alpha^\pm \ell_\beta^\pm$ and $4j$ should both equal the mass of Δ^{++}. Here, on the other hand, the invariant masses of two particular ℓjj subsets should produce mass peaks. As discussed in Ref. [9], if a discovery of LNV is eventually made at the LHC, this can be used to distinguish different models.

More important for our forecasts is, however, that the information from neutrino oscillation experiments is not sufficient to fix all entries in the Yukawa matrices $Y_{1,2,3}$. The large mixing angles observed indicate that lepton flavor violating final states should be large in $\ell_\alpha^\pm \ell_\beta^\pm + 4j$. On the other hand, the sensitivity of the LHC to final states involving tau leptons is markedly less than for muons or electrons. We thus decided to consider in our numerical studies only three simple benchmark scenarios for the Yukawa couplings. These are

(1) The scalar leptoquark couples to electrons only, i.e., $(Y_1)_{\mu\beta} = (Y_1)_{\tau\beta} = (Y_3)_{\mu\beta} = (Y_3)_{\tau\beta} = 0$.
(2) The scalar leptoquark couples to muons only, i.e., $(Y_1)_{e\beta} = (Y_1)_{\tau\beta} = (Y_3)_{e\beta} = (Y_3)_{\tau\beta} = 0$.
(3) The scalar leptoquark couples to electrons and muons (no taus) with the same rate, i.e., $(Y_1)_\mu = (Y_1)_e$, $(Y_3)_{\mu\beta} = (Y_3)_{e\beta}$ with $(Y_1)_{\tau\beta} = (Y_3)_{\tau\beta} = 0$.

Couplings to the third generation quarks could be sizeable, leading to final states involving bottom or even top quarks. However, we will limit ourselves in this paper to the study of light quarks; i.e., we consider only jets without any flavor tags for the quarks.

We close this section with the short comment that a number of similar LNV models can easily be constructed, all of which lead in principle to the same LHC signal. In fact, the model we have considered in this section corresponds to a particular example of a $d = 9$ short-range neutrinoless double beta decay operator decomposition that generates neutrino masses at two loops. As can be seen in Table IV of Ref. [30], all models in this class have an exotic colored fermion that might be pair produced at the LHC.

III. MONTE CARLO SIMULATION

In order to estimate the sensitivity reach of our model at the LHC Run 3 (i.e., an integrated luminosity of 300/fb and a center-of-mass energy of $\sqrt{s} = 13$ TeV), we have performed realistic detector level simulations of the same-sign (SS) dilepton plus four hard jets final state signal, shown

in Fig. 2, as well as of the most relevant SM backgrounds. Our signals correspond to the three benchmark scenarios described in Sec. II with the mass of the color-octet fermion m_Ψ varying in the range [1.5, 2.9] TeV, while the scalar leptoquark mass is supposed to always be larger than m_Ψ and is therefore off shell in the Ψ decay. Signal and SM background events were generated at parton level using MADGRAPH5 version 2.3.3 [31].

For the simulation of the signal, we wrote a private model file and implemented it in SARAH [32,33]. SARAH then allowed us to generate automatically a version of SPHENO [34,35], with which a numerical calculation for different observables, such as masses and decay branching ratios, can be done.

For the SM processes, we used the built-in model available in MADGRAPH, including the backgrounds $t\bar{t}, Z, W^\pm W^\pm, ZZ, ZW^\pm, W^\pm W^\mp, t\bar{t}Z, t\bar{t}W^\pm$ plus two to four additional final state partons and Z, W, and t decaying to leptons (e, μ). Parton showers and particle decays were generated with PYTHIA6.4 [36,37], and the matrix element to parton shower matching procedure (MLM) [38,39] was implemented when generating SM background processes in order to avoid double counting of the radiated partons. The interaction of final state particles with the detector and their reconstruction was simulated using DELPHES3 [40], configured to replicate the ATLAS detector layout and its performance. Jets were reconstructed with the anti-k_t algorithm using a cone size of $R = 0.4$. Note that most of the SM background processes listed above produce opposite-sign (OS) dilepton final states, while we consider only SS dilepton final states in our analysis. We must include these processes when we have final states containing electrons, due to the charge flip effect.[4] We expect indeed a significant OS event contamination into the SS region. In order to account for this effect in final states containing electrons, we reweighted our events using the charge flip probability measured by ATLAS (see Fig. 2(a) of Ref. [41]), parametrized in electron p_T and η. We did not consider background contributions from QCD jets faking leptons in our analysis, since we expect these to be negligible for very high-p_T electrons and muons, as those produced in our signal.

In order to validate our simulated SM backgrounds against measured quantities, we used those already performed at the LHC Run 2 by ATLAS and compared the simulated distribution of number of jets for $t\bar{t}$ and $Z+$jets with the measurements performed in Refs. [42] and [43], respectively. After a simple linear rescaling of the simulated distributions to the partial Run 2 luminosities and applying the selection cuts used in those studies, we compared our number of jets distributions with the distributions measured by ATLAS and derived the correction factors needed to account for the observed differences. The correction was applied to our simulated $Z+$jets and $t\bar{t}$ samples as a function of the number of jets before the preselection used in this analysis. Other samples were not corrected in this way since the corresponding measurements were not available. The preselection cuts we applied were similar for all final states considered:

(1) A pair of SS reconstructed leptons with $p_T > 20$ GeV.
(2) In the case of ee final state, we also require the dilepton mass to be larger than 110 GeV, in order to further suppress $Z + jets$ background.
(3) At least four jets are required, each of them satisfying $p_T^j > 20$ GeV.

For a discriminating variable, we used the scalar sum of the hardest leptons and jets in the event, $H_T \equiv p_T^{\ell_1} + p_T^{\ell_2} + p_T^{j_1} + p_T^{j_2} + p_T^{j_3} + p_T^{j_4}$. We found the significance is larger when using H_T compared with $m_{\ell jj}$ or $m_{\ell\ell jjjj}$ invariant mass distributions, which are both affected by a large combinatorial background, due to the many ways the jets can be paired with the leptons. H_T distributions after preselection for ee, $\mu\mu$ are shown in Fig. 3 and for $e\mu$ are shown in Fig. 4.

IV. RESULTS

In this section, we use the results from Sec. III to estimate future limits on the $\Psi \to \ell jj$ ($\ell = e, \mu$) branching fraction, for each of the benchmark scenarios described in Sec. II. Figures 3 and 4 show the number of signal and background events, before the H_T cut, for the $e^\pm e^\pm jjjj$, $\mu^\pm\mu^\pm jjjj$, and $e^\pm\mu^\pm jjjj$ final states. Depending on the final state, the signals are shown for the scenarios where the scalar leptoquark couples to electrons only (ee), muons only ($\mu\mu$), or to electrons and muons with the same strength ($e\mu$).

While the ee ($\mu\mu$) scenario is constrained by the $e^\pm e^\pm jjjj$ ($\mu^\pm\mu^\pm jjjj$) final state only, the $e\mu$ scenario is constrained by the three final states: $e^\pm e^\pm jjjj$, $\mu^\pm\mu^\pm jjjj$, and $e^\pm\mu^\pm jjjj$. For an off-shell scalar leptoquark ($S_{\rm LQ}$), the number of signal events is given by

$$S = \sigma(gg \to \Psi\Psi) \times \mathrm{Br}(\Psi \to \ell jj) \times \mathrm{Br}(\Psi \to \ell' jj) \times \mathcal{L}_{\rm int} \times \eta, \quad (3)$$

where $\ell, \ell' = e,\ \mu$, $\mathcal{L}_{\rm int} = 300\ \mathrm{fb}^{-1}$, and η is our cut efficiency. (See the discussion in the previous section and the Tables I–III in the Appendix.)

The number of signal events for both the ee and $\mu\mu$ scenarios were obtained assuming $\mathrm{Br}(\Psi \to \ell jj) = 1$, while for the $e\mu$ scenario, we assumed $\mathrm{Br}(\Psi \to ejj) = \mathrm{Br}(\Psi \to \mu jj) = 1/2$. In order to find the discovery reach and forecasted limits, we scale these results accordingly and find the minimum value of the branching ratio required

[4] In which the electron charge is wrongly tagged, an effect caused by electron-positron pair production in hard bremsstrahlung radiation emission.

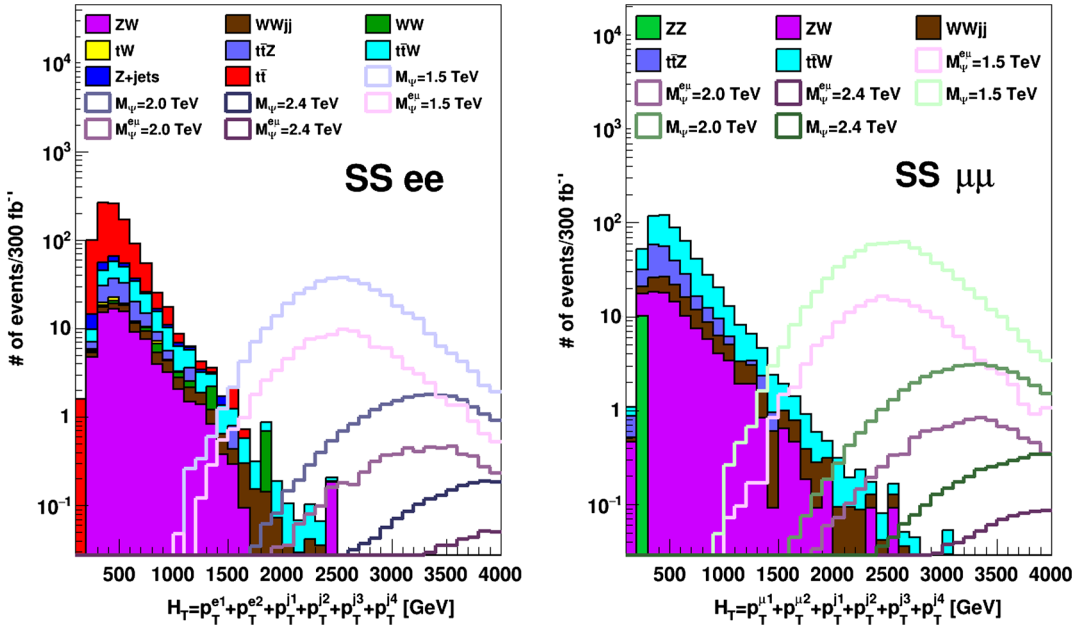

FIG. 3. Signal (solid lines) and SM background (stacked histograms) H_T^{ll} distributions after the preselection cuts described in the text are applied. Signal samples for the ee (left), $\mu\mu$ (right), and $e\mu$ (both plots) scenarios are shown. Only a few signal mass points are shown for the sake of clarity.

to get a 5σ or 2σ significance. For the significance, Z, we use the expression

$$Z = \sqrt{2\left[(S+B)\times \ln\left(1+\frac{S}{B}\right) - S\right]}, \qquad (4)$$

where S is the number of signal events and B is the number of background events. We restrict our analysis to regions with at least one signal event.

Our results are shown in Figs. 5 and 6. The three different plots correspond to the three different scenarios previously discussed: ee, $\mu\mu$, and $e\mu$. In each plot, we show the minimum branching fraction for 5σ-discovery (solid lines) and 2σ-limits (dashed lines) as a function of the mass of the color-octet fermion Ψ. From these plots, one can see that larger values of the H_T cut give better sensitivities in regions of parameter space with larger values of m_Ψ (removing most of the backgrounds), while lower values of H_T are better for smaller values of m_Ψ. For this reason, for each scenario, we show our results for two different values of the H_T cut. As expected, for high (low) masses, the expected limits are stronger (weaker) for lower (higher) values of H_T. Depending on the scenario, the LHC with 300/fb should be able to discover (give limits for) the color-octet fermion with masses in the range 2.3–2.4 TeV (2.6–2.7 TeV).

Before closing, we want to briefly discuss the LNV searches by CMS [15] and ATLAS [16], cited in the Introduction. Both experiments search for $\ell^\pm\ell^\pm jj$ final states. Since kinematics and backgrounds are different in this search relative to the $2\ell 4j$ signal that we are interested in, limits from these searches cannot be straightforwardly converted into limits on the model considered in this paper. Based on cross sections alone, from the limits given in

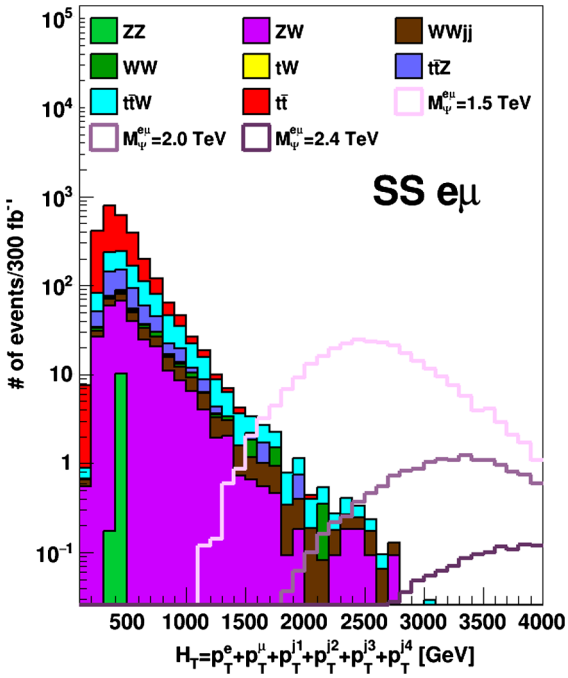

FIG. 4. Signal (solid lines) and SM background (stacked histograms) $H_T^{e\mu}$ distributions after the preselection cuts described in the text are applied. Only a few signal mass points are shown for the sake of clarity.

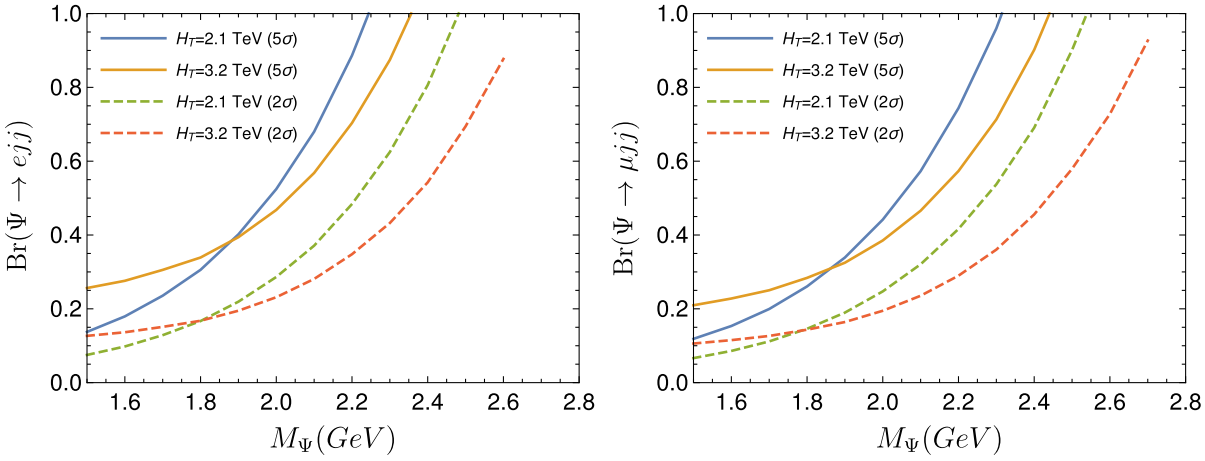

FIG. 5. Minimum $\mathrm{Br}(\Psi \to \ell jj)$ for discovery (solid lines) and 2σ-limits (dashed lines) as a function of m_Ψ, for two values of the H_T cut. Left for $\ell = e$ (in the scenario where the scalar leptoquark couples to electrons only) and right for $\ell = \mu$ (in the scenario where the scalar leptoquark couples to muons only). The red dashed line does not reach $\mathrm{Br} = 1$ because we restrict the curves to regions with more than one signal event.

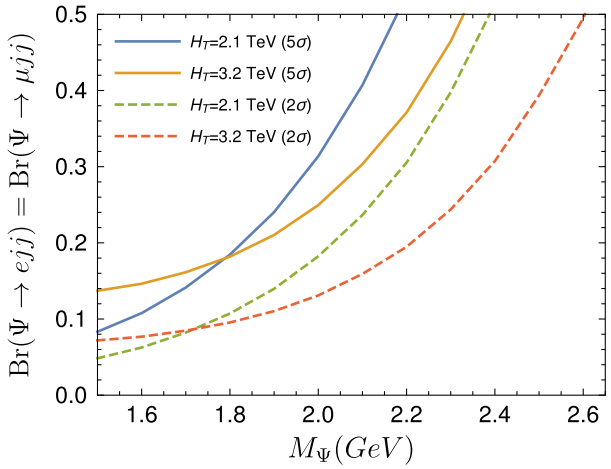

FIG. 6. Minimum $\mathrm{Br}(\Psi \to ejj) = \mathrm{Br}(\Psi \to \mu jj)$ for discovery (solid lines) and 2σ-limits (dashed lines) as a function of m_Ψ, for two values of the H_T cut, in the scenario where the scalar leptoquark couples to electrons and muons with the same strength.

Fig. 5 of Ref. [15], we guesstimate that these searches should be able to probe colored octet masses roughly up to $m_\Psi \sim 2$ TeV. We want to stress, however, that only a dedicated analysis by the experimental collaborations can derive the correct limits. Thus, there is ample room for improving the LHC searches for the LNV model studied in this paper.

V. CONCLUSIONS

We have studied the potential of the LHC Run 3 to probe lepton number violation. For our numerical study, we have used a particular two-loop neutrino mass model. We focused on a model variant in which the standard model is extended with two new particles, both singlet under the SU(2) group: a color-triplet scalar leptoquark S_{LQ} and a Majorana color-octet fermion Ψ. This model is one example of a model class with a LNV signal at the LHC consisting of same-sign dileptons plus four jets.

We have considered three different benchmark scenarios to take into account different lepton flavor signals at the LHC:

(1) S_{LQ} couples to electrons only,
(2) S_{LQ} couples to muons only, and
(3) S_{LQ} couples to electrons and muons with the same strength.

In view of the large neutrino mixing angles observed in neutrino oscillation experiments, one expects benchmark 3 to be the most realistic one. In order to estimate the sensitivity reach for the LHC, we have performed realistic detector level simulations for the signal as well as for the most relevant SM backgrounds. We have found that the LHC should be able to discover the color-octet fermion up to masses in the range (2.3–2.4) TeV or derive limits on this model up to masses order (2.6–2.7) TeV, the exact number depending on the lepton flavor composition of the final states.

In closing, we would like to point out again that this model is one example from a large class of models in which the kinematics is different from the one used by ATLAS [16] and CMS [15] searches for LNV in the left-right symmetric model. Whereas in the left-right model $p^2_{\ell\ell jj}$ should peak at the mass of the W_R, in the model we have discussed, the colored octets are pair produced, and each decays to ℓjj. Thus, there is no "mass peak" in the $p^2_{\ell\ell 4j}$ distribution. Instead, we found that the maximum sensitivity for the LHC can be obtained from studying the variable H_T, as discussed in Sec. III.

ACKNOWLEDGMENTS

E. C. is supported by FONDECYT (Chile) Grant No. 11140549 and in part by CONICYT Basal Grant No. FB0821. M. H. is supported by the Spanish Grants No. SEV-2014-0398 and No. FPA2017-85216-P (AEI/FEDER, UE) and No. PROMETEO/2018/165 (Generalitat Valenciana). J. C. H. is supported by FONDECYT Grant No. 1161463. N. N. was supported by FONDECYT Grant No. 3170906 and in part by Conicyt PIA/Basal Grant No. FB0821.

APPENDIX: CUT FLOW RESULTS, EVENT YIELDS

In this section, we include the expected (simulated) signal and background yields (weighted for 300/fb) for the cut based analysis developed in this work. The tables are organized as follows: signal and background yields are separated by the horizontal line at mid-height and above and below, respectively. The first column labels the generated processes, the signal points are labeled by the Ψ mass, and the scenario is shown between parentheses. Numbers are quoted for only a few signal mass points. The second column contains the expected number of events at the target integrated luminosity ($\mathcal{L}_{\rm int} = 300/\text{fb}$), calculated using the cross section obtained with MadGraph (σ_{MG}) for each process. The subsequent columns show the remaining event yields after each preselection cut is applied (see Sec. III), while the last two columns correspond to the looser and harder H_T cuts, respectively. After column 3, the event yields also contain the different corrections applied as explained in Sec. III.

TABLE I. Cut flow table showing event yields for signal and SM background processes in the $eejjjj$ final state.

m_ψ TeV (scenario)	$\sigma_{\rm MG} \times \mathcal{L}_{\rm int}$	ee	$\ell^\pm\ell^\pm$	≥ 4 jets	$m_{ee} > 110$ GeV	$H_T > 2.1$ TeV	$H_T > 3.2$ TeV
2.4 ($e\mu$)	18.05	1.60	0.80	0.79	0.78	0.78	0.68
2.0 ($e\mu$)	146.33	13.07	6.53	6.45	6.41	6.31	3.82
1.5 ($e\mu$)	2395.50	218.31	109.16	107.48	106.04	90.98	13.44
2.4 (ee)	18.11	6.43	3.21	3.17	3.15	3.14	2.76
2.0 (ee)	146.64	51.72	25.86	25.50	25.29	24.93	15.18
1.5 (ee)	2396.69	867.22	433.61	427.69	421.70	362.93	50.62
ZZ	3.36×10^6	4.99×10^4	1037.84	42.63	0.00	0.00	0.00
ZW	7.29×10^4	9537.70	2631.64	148.83	82.36	0.18	0.00
$WWjj$	2059.42	151.19	151.19	26.62	18.43	0.14	0.01
WW	5.58×10^6	6.84×10^4	820.77	13.67	8.24	0.00	0.00
tW	1.09×10^6	1.81×10^4	170.38	6.22	4.71	0.00	0.00
$t\bar{t}Z$	1.76×10^5	1879.39	172.93	113.13	57.22	0.00	0.00
$t\bar{t}W$	4920.41	354.99	303.27	168.71	98.96	0.22	0.02
Z + jets	6.35×10^6	2.76×10^6	2.90×10^4	112.74	34.81	0.00	0.00
$t\bar{t}$	8.28×10^6	4.94×10^5	4423.30	1204.54	709.53	0.00	0.00
Total background	2.49×10^7	3.40×10^6	3.87×10^4	1837.10	1014.26	0.54	0.03

TABLE II. Cut flow table showing event yields for signal and SM background processes in the $\mu\mu jjjj$ final state.

m_ψ TeV (scenario)	$\sigma_{\rm MG} \times \mathcal{L}_{\rm int}$	$\mu\mu$	$\ell^\pm\ell^\pm$	≥ 4 jets	$H_T > 2.1$ TeV	$H_T > 3.2$ TeV
2.4 ($\mu\mu$)	18.10	11.54	5.77	5.69	5.66	4.84
2.0 ($\mu\mu$)	146.62	90.94	45.47	44.94	44.19	25.97
1.5 ($\mu\mu$)	2399.39	1459.49	729.75	720.87	612.38	87.69
2.4 ($e\mu$)	18.05	2.79	1.39	1.37	1.37	1.18
2.0 ($e\mu$)	146.33	22.70	11.35	11.22	11.02	6.50
1.5 ($e\mu$)	2395.50	365.15	182.57	180.08	152.73	20.46
ZZ	3.36×10^6	8.56×10^4	529.97	10.19	0.00	0.00
ZW	7.29×10^4	1.14×10^4	2157.96	95.70	0.18	0.00
$WWjj$	2059.42	263.06	263.06	49.24	0.42	0.03
$t\bar{t}Z$	1.76×10^5	3052.49	192.12	115.90	0.00	0.00
$t\bar{t}W$	4920.41	621.46	530.48	301.92	0.50	0.03
Total background	3.62×10^6	1.01×10^5	3673.59	572.96	1.11	0.06

TABLE III. Cut flow table showing event yields for signal and SM background processes in the $e\mu jjjj$ final state.

m_ψ TeV (scenario)	$\sigma_{\mathrm{MG}} \times \mathcal{L}_{\mathrm{int}}$	$e\mu$	$\ell^\pm\ell^\pm$	≥ 4 jets	$H_T > 2.1$ TeV	$H_T > 3.2$ TeV
2.4 ($e\mu$)	18.05	4.29	2.15	2.12	2.11	1.81
2.0 ($e\mu$)	146.33	33.72	16.86	16.69	16.43	9.86
1.5 ($e\mu$)	2395.50	559.55	279.78	275.97	235.27	32.98
ZZ	3.36×10^6	2293.14	855.36	10.40	0.00	0.00
ZW	7.29×10^4	9895.41	5017.54	264.76	0.65	0.00
$WWjj$	2059.42	399.49	399.49	72.20	0.58	0.04
WW	5.58×10^6	1.79×10^5	1076.52	23.70	0.27	0.00
tW	1.09×10^6	4.61×10^4	246.09	11.85	0.00	0.00
$t\bar{t}Z$	1.76×10^5	1960.52	365.72	237.08	0.00	0.00
$t\bar{t}W$	4920.41	938.40	802.70	453.05	0.69	0.05
$t\bar{t}$	8.28×10^6	1.28×10^6	6065.34	1651.22	0.00	0.00
Total background	1.86×10^7	1.52×10^6	1.48×10^4	2724.25	2.18	0.09

[1] J. C. Pati and A. Salam, Phys. Rev. D **10**, 275 (1974).
[2] R. Mohapatra and J. C. Pati, Phys. Rev. D **11**, 2558 (1975).
[3] R. N. Mohapatra and G. Senjanovic, Phys. Rev. D **23**, 165 (1981).
[4] W.-Y. Keung and G. Senjanovic, Phys. Rev. Lett. **50**, 1427 (1983).
[5] V. Tello, M. Nemevsek, F. Nesti, G. Senjanovic, and F. Vissani, Phys. Rev. Lett. **106**, 151801 (2011).
[6] F. Bonnet, M. Hirsch, T. Ota, and W. Winter, J. High Energy Phys. 03 (2013) 055.
[7] P. F. de Salas, D. V. Forero, C. A. Ternes, M. Tortola, and J. W. F. Valle, Phys. Lett. B **782**, 633 (2018).
[8] J. C. Helo, M. Hirsch, S. G. Kovalenko, and H. Päs, Phys. Rev. D **88**, 011901(R) (2013).
[9] J. C. Helo, S. G. Kovalenko, M. Hirsch, and H. Päs, Phys. Rev. D **88**, 073011 (2013).
[10] L. Gonzales, J. C. Helo, M. Hirsch, and S. G. Kovalenko, J. High Energy Phys. 12 (2016) 130.
[11] P. F. Perez and M. B. Wise, Phys. Rev. D **80**, 053006 (2009).
[12] P. F. Perez, T. Han, S. Spinner, and M. K. Trenkel, J. High Energy Phys. 01 (2011) 046.
[13] V. Khachatryan *et al.* (CMS Collaboration), Eur. Phys. J. C **74**, 3149 (2014).
[14] G. Anamiati, M. Hirsch, and E. Nardi, J. High Energy Phys. 10 (2016) 010.
[15] A. M. Sirunyan *et al.* (CMS Collaboration), J. High Energy Phys. 05 (2018) 148.
[16] M. Aaboud *et al.* (ATLAS Collaboration), J. High Energy Phys. 01 (2019) 016.
[17] G. Azuelos, K. Benslama, and J. Ferland, J. Phys. G **32**, 73 (2006).
[18] P. F. Perez, T. Han, G.-y. Huang, T. Li, and K. Wang, Phys. Rev. D **78**, 015018 (2008).
[19] A. Melfo, M. Nemevsek, F. Nesti, G. Senjanovic, and Y. Zhang, Phys. Rev. D **85**, 055018 (2012).
[20] F. del Aguila, M. Chala, A. Santamaria, and J. Wudka, Phys. Lett. B **725**, 310 (2013).
[21] M. Aaboud *et al.* (ATLAS Collaboration), Eur. Phys. J. C **78**, 199 (2018).
[22] M. Aaboud *et al.* (ATLAS Collaboration), Eur. Phys. J. C **79**, 58 (2019).
[23] A. M. Sirunyan *et al.* (CMS Collaboration), Phys. Rev. D **99**, 052002 (2019).
[24] M. Aaboud *et al.* (ATLAS Collaboration), arXiv:1902.00377.
[25] K. Babu and C. N. Leung, Nucl. Phys. **B619**, 667 (2001).
[26] P. W. Angel, Y. Cai, N. L. Rodd, M. A. Schmidt, and R. R. Volkas, J. High Energy Phys. 10 (2013) 118.
[27] I. Baldes, N. F. Bell, and R. R. Volkas, Phys. Rev. D **84**, 115019 (2011).
[28] A. de Gouvea and J. Jenkins, Phys. Rev. D **77**, 013008 (2008).
[29] D. A. Sierra, A. Degee, L. Dorame, and M. Hirsch, J. High Energy Phys. 03 (2015) 040.
[30] J. C. Helo, M. Hirsch, T. Ota, and F. A. P. dos Santos, J. High Energy Phys. 05 (**2015**) 092.
[31] J. Alwall, M. Herquet, F. Maltoni, O. Mattelaer, and T. Stelzer, J. High Energy Phys. 06 (2011) 128.
[32] F. Staub, Comput. Phys. Commun. **184**, 1792 (2013).
[33] F. Staub, Comput. Phys. Commun. **185**, 1773 (2014).
[34] W. Porod, Comput. Phys. Commun. **153**, 275 (2003).
[35] W. Porod and F. Staub, Comput. Phys. Commun. **183**, 2458 (2012).
[36] T. Sjostrand, P. Edén, C. Friberg, L. Lönnblad, G. Miu, S. Mrenna, and E. Norrbin, Comput. Phys. Commun. **135**, 238 (2001).
[37] T. Sjostrand, S. Mrenna, and P. Z. Skands, J. High Energy Phys. 05 (2006) 026.

[38] M. Mangano, in *Proceedings of the Fermilab ME/MC Tuning Workshop* (2002).
[39] M. L. Mangano, M. Moretti, F. Piccinini, and M. Treccani, J. High Energy Phys. 01 (2007) 013.
[40] S. Ovyn, X. Rouby, and V. Lemaitre, arXiv:0903.2225.
[41] ATLAS and T. A. Collaboration, CERN Report No. ATLAS-CONF-2013-051, 2013.
[42] M. Aaboud *et al.* (ATLAS Collaboration), Phys. Lett. B **761**, 136 (2016); **772**, 879(E) (2017).
[43] M. Aaboud *et al.* (ATLAS Collaboration), Eur. Phys. J. C **77**, 361 (2017).